A novel connection between *Trypanosoma brucei* mitochondrial proteins TbTim17 and TbTRAP1 is discovered using Biotinylation Identification (BioID)

Fidel Soto-Gonzalez, Anuj Tripathi, Ayorinde Cooley, Victor Paromov, Tanu Rana, and Minu Chaudhuri*
From the Department of Microbiology, Immunology, and Physiology, School of Medicine, Meharry Medical College, Nashville, Tennessee, USA

Edited by Ruma Banerjee

The protein translocase of the mitochondrial inner membrane in *Trypanosoma brucei*, TbTIM17, forms a modular complex in association with several other trypanosome-specific proteins. To identify transiently interacting proximal partner(s) of TbTim17, we used Biotinylation Identification (BioID) by expressing a modified biotin ligase-TbTim17 (BirA*-TbTim17) fusion protein in *T. brucei*. BirA*-TbTim17 was targeted to mitochondria and assembled in the TbTIM complex. In the presence of biotin, BirA*-TbTim17 biotinylated several mitochondrial proteins. Interestingly, TbHsp84/TbTRAP1, a mitochondrial Hsp90 homolog, was identified as the highest enriched biotinylated proteins. We validated that interaction and colocalization of TbTim17 and TbHsp84 in *T. brucei* mitochondria by coimmunoprecipitation analysis and confocal microscopy, respectively. TbTim17 association with TbTRAP1 increased several folds during denaturation/renaturation of mitochondrial proteins *in vitro*, suggesting TbTRAP1 acts as a chaperone for TbTim17 refolding. We demonstrated that knockdown of TbTRAP1 reduced cell growth and decreased the levels of the TbTIM17, TbTim62, and mitochondrial (m)Hsp70 complexes. However, ATPase, VDAC, and Atom69 complexes were minimally affected. Additionally, the steady state levels of TbTim17, TbTim62, and mHsp70 were reduced significantly, but Atom69, ATPase β, and RBP16 were mostly unaltered due to TbTRAP1 knockdown. Quantitative proteomics analysis also showed significant reduction of TbTim62 along with a few other mitochondrial proteins due to TbTRAP1 knockdown. Finally, TbTRAP1 depletion did not hamper the import of the ectopically expressed TbTim17-2xMyc into mitochondria but reduced its assembly into the TbTIM17 complex, indicating TbTRAP1 is critical for assembly of TbTim17. This is the first report showing the role of TRAP1 in the TIM complex assembly in eukaryotes.

The flagellated protozoan parasite *Trypanosoma brucei* (*T. brucei*) possesses a single mitochondrion per cell and has a complex concatenated disk-like structure of mitochondrial DNA known as the kinetoplast (1). Therefore, this group of parasites is known as Kinetoplastida (2). Various species within the class Kinetoplastea cause serious diseases in humans worldwide, such as African Trypanosomiasis (AT), Chagas disease, and leishmaniasis (3–5). *T. brucei* subspecies cause AT, a fatal disease in humans as well as in domestic animals. AT is endemic in sub-Saharan Africa, the habitat of the tsetse fly, which is the transmission vector for this parasite (6). Despite an elaborate mitochondrial DNA structure, the *T. brucei* mitochondrion encodes only 18 proteins. Thus, as with other eukaryotes, trypanosomes import 99% of mitochondrial proteins from the cytosol (7, 8).

Previous discoveries revealed that mitochondrial protein import machinery in trypanosomatids is significantly divergent in comparison to that in well-studied organisms, such as fungi, mammals, and plants, which belong to the eukaryotic supergroup Opisthokonta and Archeplastida, respectively (8–12). In these groups, most of the mitochondrial proteins use the translocase of the mitochondrial outer membrane (TOM) complex to enter mitochondria (13). Once across the mitochondrial outer membrane, these proteins are sorted into two different translocases of the mitochondrial inner membrane (MIM) (TIM23 and TIM22) to be destined to the mitochondrial matrix, MIM, and the intermembrane space (IMS) (9, 10). In general, the N-terminal signal-containing matrix proteins and a few MIM proteins with an additional sorting signal are transported through the TIM23 complex (14–16), whereas the hydrophobic inner membrane proteins with internal targeting signals are sorted through the TIM22 complex (17, 18). The TOM and TIMs are multiprotein complexes, and subunits overall are conserved in these groups, although variations of components exist among different species. In contrast, trypanosomatids belong to the supergroup Excavatae and diverged very early during evolution. Trypanosomatids possess an archaic TOM (ATOM) complex and a single TIM complex, the TbTIM17 translocase (19, 20). Although the pore-forming subunit of the ATOM and TOM, Atom40 and Tom40, respectively, are homologous, the other ATOM subunits, Atom11, Atom12, Atom14, and Atom19, are distinctly trypanosome specific (21). Two receptor subunits,

Atom46 and Atom69, are distantly related to Tom20 and Tom70 of the TOM complex, respectively (22).

The major component of the TbTIM17 complex is TbTim17 with a predicted size 16.3 kDa. TbTim17 is homologous to the pore-forming subunits of the TIM23 (Tim23 and Tim17) and TIM22 (Tim22) complexes (20, 23). As reported so far, TbTim17 associates with TbTim62, TbTim42, six small TbTims, Rhomboid I (Rhom I), Rhomboid II (Rhom II), acyl CoA dehydrogenase (ACAD), TbTim50, and TbTim54 (20, 23–28). However, the overall structure of the TbTIM17 complex is elusive. Blue-native (BN)-PAGE revealed that TbTIM17 forms modular complexes within the range of 300 kDa to >800 kDa (29). TbTim62 primarily is found in a ~150 kDa complex with a fraction of TbTim17 (30). All six small TbTims (TbTim9, TbTim10, TbTim11, TbTim12, TbTim13, and TbTim8/13) are associated stably with TbTim17 (27, 28). Excluding TbTim17, TbTim50, and few small TbTims, all other components of the TbTIM17 complex are unique to trypanosomes. As in other eukaryotes, *T. brucei* nuclear-encoded mitochondrial proteins possess either N-terminal or internal targeting signals (7, 8). Surprisingly, TbTIM17 is capable of sorting both types of targeting signal-containing proteins to submitochondrial destinations (24). It is postulated that TbTim17 dynamically associates with different subunits to form modular complexes to perform this job; however, the exact mechanism has not been elucidated yet.

As the approaches that have been used to characterize the TbTIM17 complex may overlook weak/transient interactions, we used the Biotinylation Identification (BioID) technique to identify TbTim17 proximal proteins. In this approach, a bait protein is fused in frame with a mutated form of the biotin ligase from *Escherichia coli* (BirA*) (31) and expressed in the target cells. BirA* biotinylates lysine residues on a neighboring protein (~10 nm distance), enabling the purification of close-proximity proteins (31, 32). Once biotinylated, proteins are extracted from cells under stringent denaturing conditions, recovered by streptavidin affinity purification, and identified by mass spectrometry (MS) (31, 32). Despite the advantages of the BioID approach, the techniques have not yet been applied for characterization of the TbTIM17 complex from *T. brucei*.

We employed the BioID approach using TbTim17, the main component of the TbTIM complex as bait. We identified a few previously confirmed interacting proteins of TbTim17, as well as several additional candidates. One of the top-hit candidates was mitochondrial heat-shock protein 84 (Hsp84), a member of the Hsp90 family and known as TbTRAP1. A recent study showed that TbTRAP1 is involved in the kinetoplast replication in *T. brucei* (33). However, no previous reports exist of interaction between TbTim17 and TbTRAP1. TRAP1 functions have been studied in greater detail in humans (34–38). TRAP1 knockdown increases oxidative phosphorylation (39). TRAP1 is upregulated in many types of cancer cells, where it promotes glycolysis and reduces the OXPHOS pathway of ATP generation (36). Therefore, production of reactive oxygen species is reduced by the increased levels of NADPH, and cells become more resistant to apoptosis (36). Other studies showed

that TRAP1 depletion increases glutamine metabolism to increase oxidative phosphorylation and an increase in GSH levels reduces reactive oxygen species in these cells (39). Bacterial homolog of Hsp90, HtpG, is also a conserved and abundant protein (40). It has been shown that HtpG acts in cooperation with bacterial Hsp70, DnaK, to protect proteins from aggregation and helps to fold proteins properly to form large complexes, like the phycobilisome in cyanobacteria (41). Here, we identified TbTRAP1 as an interacting partner of TbTim17 and showed that TbTRAP1 is required for TbTim17 complex assembly. Knockdown of TbTRAP1 not only reduced the levels of the TbTIM17 complex but also decreased the levels of TbTim17, TbTim62, and mHsp70, the core components of the TbTIM17 complex. Some of the higher molecular mass protein complexes of mHsp70 were also severely affected by TbTRAP1 knockdown. Furthermore, TbTRAP1 depletion did not hamper the import of the ectopically expressed TbTim17-2xMyc into *T. brucei* mitochondria but reduced its assembly into the TbTIM17 complex. Therefore, TbTRAP1 appears to act in cooperation with mHsp70 for formation of the TbTIM complex in *T. brucei*, thus essential for cell growth.

Results

BirA*-TbTim17 is localized in mitochondria and assembled in the TbTIM17 complex in T. brucei

As in other Tim17/22/23 family proteins, TbTim17 has four predicted transmembrane domains with hydrophilic N- and C-terminal domains exposed in the IMS (42). Similar to other family members, TbTim17 does not have an N-terminal mitochondrial targeting signal but uses internal targeting signals for its entry into mitochondria (29), suggesting that tagging at the N-terminal of TbTim17 would not prevent its localization into mitochondria. Therefore, we generated an N-terminally BirA*-tagged TbTim17 construct using the pLew-Myc-BirA expression vector (Fig. 1A) and developed a stable *T. brucei* cell line (BirA*-TbTim17) to express this fusion protein. We performed immunoblot analysis with BirA antibody of total cellular proteins harvested at different time points (0 h–96 h) after induction of expression by addition of doxycycline in the medium. We observed that BirA*-TbTim17 is expressed at expected size (~50 kDa), and maximum level of expression was within 24 h to 72 h (Fig. S1). We verified that expression of BirA*-TbTim17 caused no adverse effects on cell growth (Fig. 1B).

Next, we harvested cells after 24 h of induction and performed cell fractionation to separate mitochondrial and cytosolic fractions. Analysis of the total, cytosolic, and mitochondrial fractions by immunoblot analysis using BirA antibody showed that BirA*-TbTim17 is present in the total and mitochondrial fraction (Fig. 1C). To verify the specificity of the antibody, we analyzed similar fractions from the parental *T. brucei* and did not observe any bands, as expected. Probing the blot with TbTim17 antibody showed the presence of endogenous TbTim17 in the total and mitochondrial fractions from both parental and BirA*-TbTim17 cell lines; however, the 50 kDa fusion protein was detected by this antibody
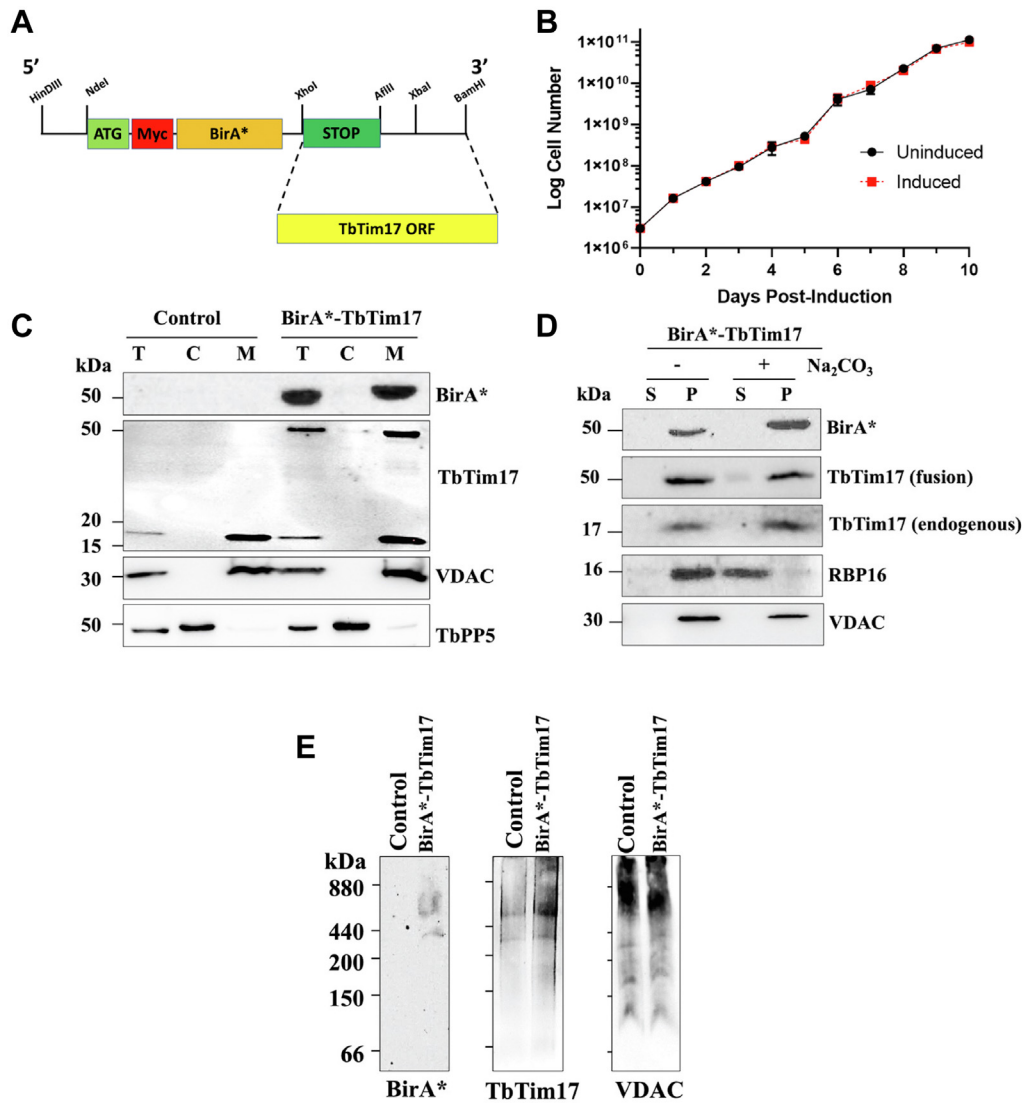
Figure 1. Expression and mitochondrial localization of the BirA*-TbTim17 fusion protein in *T. brucei*. *A*, a schematic showing the cloning strategy of the TbTim17 ORF into the modified pLew100_Myc_BirA* plasmid. Restriction sites were indicated at the *top*. *B*, growth curve for BirA*-TbTim17 cell line in the absence (uninduced) and presence (induced) of doxycycline for 10 days. The log of the cumulative cell numbers was plotted *versus* time. *C*, analysis of the subcellular fractions obtained from the parental control and BirA*-TbTim17 *T. brucei* cells grown in the presence of doxycycline for 2 days. Proteins from the total (T), cytosolic (C), and mitochondrial (M) fractions were subjected to SDS-PAGE, transferred to membrane, and probed with BirA and TbTim17 antibodies. VDAC and TbPP5 were used as the mitochondrial and cytosolic protein markers, respectively. *D*, sodium carbonate extraction was followed by immunoblot analysis of mitochondrial proteins from BirA*-TbTim17 *T. brucei* cells grown in the presence of doxycycline. The supernatant (S) and the pellet (P) fractions were analyzed using BirA*, TbTim17, VDAC, and RBP16 antibodies. *E*, mitochondria isolated from uninduced (Control) and induced BirA*-TbTim17 cells were solubilized with digitonin, and protein complexes were analyzed by BN-PAGE, followed by immunoblotting with BirA* (*left*), TbTim17 (*middle*), and VDAC (*right*) antibodies. BN, blue-native; VDAC, voltage-dependent anion channel.

only from the BirA*-TbTim17 cells. The voltage-dependent anion channel (VDAC) protein and *T. brucei* protein phosphatase 5 (TbPP5) were used as markers for the mitochondrial and cytosolic fractions, respectively. *In situ* immunofluorescence studies of BirA*-TbTim17 *T. brucei* using BirA antibody showed colocalization of BirA*-TbTim17 with Mitotracker-stained mitochondria (Fig. S2). We also have attempted to express C-terminally BirA*-tagged TbTim17 (TbTim17-BirA*). However, we did not get good expression of this fusion protein, likely because the protein was not localized/assembled in mitochondria and rapidly degraded. To determine whether the N-terminally tagged BirA*-TbTim17 was integrated in the mitochondrial membrane, isolated

mitochondria was treated with alkaline sodium carbonate, and the soluble and membrane-integral proteins were separated by centrifugation. Immunoblot analysis of the supernatant (S) and pellet (P) fractions showed that similar to the endogenous TbTim17, BirA*-TbTim17 was present in pellet fraction (Fig. 1*D*). VDAC was used as the control for another membrane integral protein, and RBP16, a matrix protein, was found in the supernatant as expected.

We also analyzed mitochondrial membrane protein complexes from the control and BirA*-TbTim17 cells by BN-PAGE, followed by immunoblot analysis using antibodies for BirA, TbTim17, and VDAC. Results showed that BirA*-TbTim17 was assembled in a higher molecular mass complex

(∼800 kDa), such as endogenous TbTim17 (Fig. 1E). BirA antibody did not detect any protein bands from the control sample. As reported previously, TbTim17 antibody detected multiple protein complexes within the range of (300 kDa to >800 kDa) from both samples. As anti-TbTim17 detected both the endogenous and the fusion proteins, the ∼800 kDa complex was detected with greater intensity in the BirA*-TbTim17 mitochondria sample than in the control. As a loading control, we probed using VDAC antibody and detected different-sized, multimeric forms of VDAC at similar intensity from both samples (Fig. 1E). Altogether, our results showed that BirA*-TbTim17 was expressed, targeted to the mitochondrial membrane, and assembled in the TbTIM17 complex.

BirA*-TbTim17 biotinylates other cellular proteins enriched in the mitochondria

Next, we investigated whether BirA*-TbTim17 biotinylates other *T. brucei* proteins. For this purpose, BirA*-TbTim17 cells were grown in the presence and absence of doxycycline, either in biotin-free (I) or regular medium (II).

After 12 h of induction, cells grown in regular medium were divided into two flasks, and in one of the flasks excess biotin (50 μM) was added (III). All cells were allowed to grow for an additional 12 h. Parental control cells also were grown under similar conditions in parallel. Next, cells were harvested, and the total, cytosolic, and mitochondrial fractions were separated. Analysis of proteins from these fractions by immunoblot using horseradish peroxidase (HRP)–conjugated streptavidin showed the presence of biotinylated proteins of different sizes in the cell lysate obtained from induced BirA*-TbTim17 cells, grown either in the normal or excess biotin-containing medium (Fig. 2A), but not in biotin-free medium. A few biotinylated proteins >100 kDa in size, which could be endogenously biotinylated proteins, were common in the control and BirA*-TbTim17–induced and BirA*-TbTim17–uninduced samples. However, multiple proteins (15 kDa to 80 kDa) detected by HRP-streptavidin were very specific for the induced BirA*-TbTim17 samples and absent either in control or uninduced cells (Fig. 2). Among these, only one or two proteins (>80 kDa) were found in the cytosolic fraction (Fig. 2B) but remaining biotinylated proteins (15 kDa to 50 kDa) were present in the mitochondrial fraction (Fig. 2C).
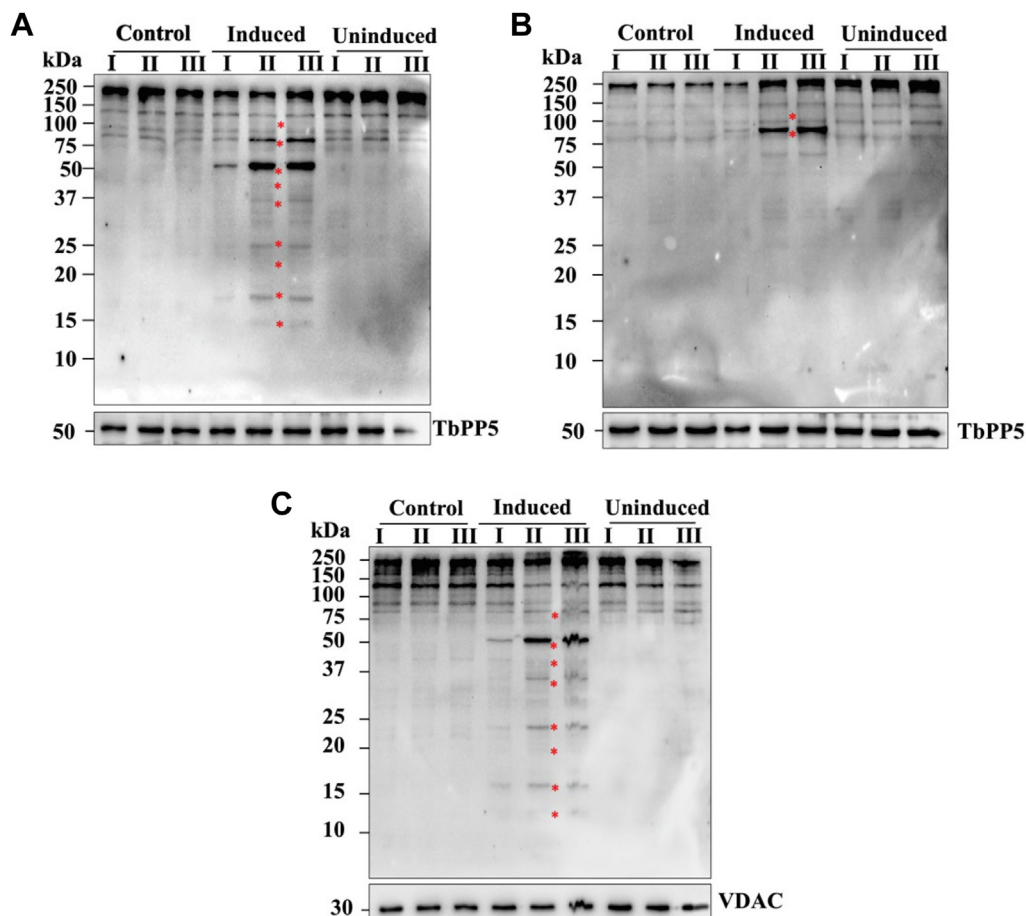

Figure 2. Biotinylation pattern of *T. brucei* proteins by BirA*-TbTim17. BirA*-TbTim17 cells were induced or kept uninduced and grown either in the absence of biotin (I) or regular (II) medium. After 12 h postinduction, cells grown in regular medium were divided into two parts, and one part was supplemented with excess biotin (III). The parental control cells also were grown in parallel under similar conditions. At 24 h postinduction, cells were harvested and subcellular fractions were separated. Immunoblots of total (*A*), cytosol (*B*), and mitochondrial (*C*) fractions were probed with HRP-conjugated streptavidin. TbPP5 and VDAC were used as the total, cytosolic, and mitochondrial protein markers, respectively. *Red asterisks* represent unique biotinylated bands compared to control and uninduced BirA*-TbTim17 samples. HRP, horseradish peroxidase; VDAC, voltage-dependent anion channel.

This demonstrated that BirA*-TbTim17 biotinylated more mitochondrial proteins, as expected. TbPP5 was used as a loading control for the total and cytosolic samples. VDAC was used as a loading control for the mitochondrial samples. A similar biotinylating pattern was observed in multiple experiments. The 50 kDa protein band could be the BirA*-TbTim17 fusion protein itself and possibly generated due to self-biotinylation. We speculated that the ~19 kDa biotinylated protein is the endogenous TbTim17, as it is present in the same complex with the fusion protein, shown in Figure 1*E*.

Purification of biotinylated proteins identifies novel proximal partners of TbTim17

We purified the biotinylated proteins from the clarified mitochondrial lysate from induced and uninduced BirA*-TbTim17 cells using Streptavidin-coupled Dynabeads. Precipitated proteins were analyzed by immunoblot using HRP-streptavidin as the probe (Fig. 3, top panel). Results showed that biotinylated proteins were purified, as these were enriched in the bound fraction from the BirA*-TbTim17–induced cells. A few biotinylated proteins of higher molecular sizes also were found in the bound fraction from the uninduced sample; however, as mentioned earlier, these could be endogenously biotinylated proteins. We observed a similar profile of the bound protein bands from three independent experiments. Reprobing this blot with BirA antibody showed that BirA*-TbTim17 was biotinylated, as it was detected in the

bound fraction from induced BirA*-TbTim17 samples only (Fig. 3, second panel). TbTim17 antibody recognized both the endogenous TbTim17 and the fusion protein, BirA*-TbTim17, in the bound fraction (Fig. 3, third panel), which further supports that these proteins were in the same complex. In contrast, VDAC and mHsp70 were only detected in the input and flow-through (unbound) fractions from both the induced and uninduced samples.

Equal amounts of purified biotinylated proteins from both uninduced and induced samples were digested with trypsin and peptide mixtures were analyzed by nano-LC-MS/MS. Mass spectra were searched against the TriTryp database (TriTrypDB). After applying the false discovery rate of <1% and at least two unique peptides for each protein, ~100 *T. brucei* proteins were identified with significant scores for each set (see Datasets S1 and S2 in the supplemental material). Data obtained from two independent biological replicates were used to estimate statistical significance. Following statistical analysis, we found 35 proteins were enriched (3- to 12-fold) in the purified biotinylated protein pools from the BirA*-TbTim17–induced *versus* BirA*-TbTim17–uninduced samples (Table 1). Among these, 17 proteins have known mitochondrial localization and 11 were uncharacterized putative proteins. Among all mitochondrial proteins, 28%, 9%, and 21% were known MIM, mitochondrial outer membrane, and matrix proteins, respectively (Fig. 4). The most enriched (10- to 12-fold) protein in the BirA*-TbTim17–induced sample was mitochondrial heat shock protein 84 (TbHsp84 or TbTRAP1) in all replicates (Table 1). Moreover, we found TbTim17, mitochondrial processing peptidase, several carrier proteins, glutathione-*S*-transferase (GST), universal minicircle binding protein, cytochrome oxidase subunit V, and cytochrome c1 in the enriched protein fraction (Table 1). Surprisingly, we did not observe many previously characterized Atom or TbTim subunits, except for Atom69, Atom46, and TbTim17. This possibly is because the lysine residues of the other TbTim17-associated proteins were not exposed and/or proximal to BirA*.

Figure 3. Purification of biotinylated proteins from BirA*-TbTim17 cells. The BirA*-TbTim17 cells were grown in the presence of doxycycline for 12 h in regular medium. Next, excess biotin (50 μM) was added to the medium, and cells were grown for an additional 12 h. Uninduced (Control) cells were grown in parallel under similar conditions. Cells were harvested, and crude mitochondrial fractions were isolated. Mitochondrial proteins were solubilized with NP-40 (1%) and used for affinity purification using Streptavidin-conjugated Dynabeads. Samples from each step of the purification process were collected for further analysis. Immunoblot analysis of the input (I), flow-through (Ft), washed (W1-W3), and bound (B) proteins were performed using streptavidin-HRP (Top panel) as the probe. Blots were reprobed with BirA*, TbTim17, VDAC, and mHsp70 antibodies. HRP, horseradish peroxidase; VDAC, voltage-dependent anion channel.

Endogenously tagged TbHSP84-3xHA is localized in the mitochondria and associates with TbTim17

Using the BioID approach, we discovered TbTRAP1 as a novel proximal partner of TbTim17. However, it was necessary to investigate whether this association occurs in cells with normal levels of TbTim17 and not due to overexpression of BirA*-TbTim17. For this purpose, we developed a *T. brucei* cell line, whereby TbTim17 and TbTRAP1 were *in situ* tagged with 6xMyc and 3xhemagglutinin (HA) epitopes at the N and C terminus (6xMyc-TbTim17 and TbTRAP1-3xHA), respectively (Fig. 5*A*). Subcellular fractionation and immunoblot analysis showed that addition of these tags did not alter their subcellular location. The 6xMyc-TbTim17 and TbTRAP1-3xHA were detected only in the total and mitochondrial fractions using anti-Myc and anti-HA antibodies, respectively (Fig. 5*B*). No band was detected with these antibodies from the parental control. We also used the *T. brucei* cell line, whereby
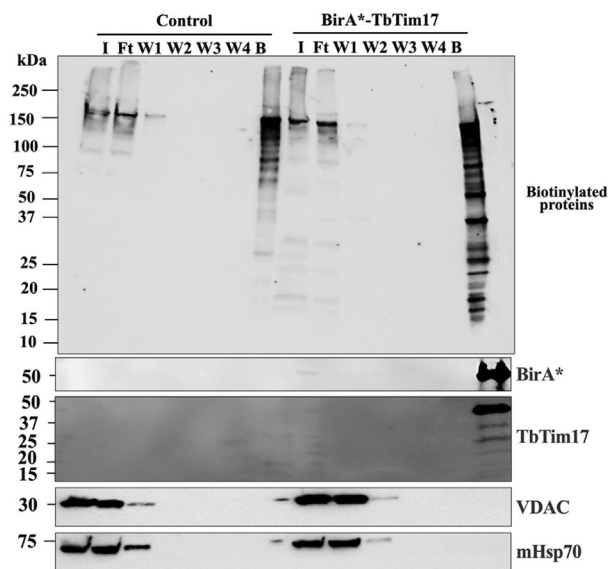
Table 1
Enriched biotinylated proteins by BirA*-TbTim17

Protein name	UniProt ID	Fold change
Heat shock protein 84, mitochondrial	Q386P5	12.75
Glutathione-S-transferase/glutaredoxin, putative	Q57WG5	12
Universal minicircle sequence binding protein (UMSBP)	Q38AZ9	12
Mitochondrial processing peptidase, beta subunit	Q57W51	8.1
Inner membrane preprotein translocase Tim17	Q382K7	8.1
Mitochondrial carrier protein, putative	Q388W2	8.1
Mitochondrial import receptor, ATOM69	Q383D2	6
Mitochondrial carrier protein, putative	Q385N9	6
Putative uncharacterized protein	Q57X78	6
Putative uncharacterized protein	Q382L8	6
Putative uncharacterized protein	Q57X97	6
Mitochondrial carrier protein, putative	Q38DX9	6
Microtubule-associated protein, putative	Q389U1	4.1
ATP synthase subunit F1	Q387C5	4
Putative uncharacterized protein	Q382G6	4
Mitochondrial import receptor, ATOM46	Q384P0	4
Putative uncharacterized protein	Q385L8	4
Protein tyrosine phosphatase, putative	Q389R7	4
Fructose-1,6-bisphosphate, cytosolic	Q38EA4	4
Cytochrome c oxidase subunit V	Q38FK9	4
Electron transport protein SCO1/SCO2	Q38FS2	4
Proline oxidase, putative	Q57U33	4
3,2-trans-enoyl-CoA isomerase, mitochondrial	Q57V74	4
Cytochrome c1, heme protein, mitochondrial	D6XKS6	4
Calpain-like protein, putative	Q4GYZ8	4
Short-chain dehydrogenase, putative	Q389B9	4
Putative uncharacterized protein	Q383R4	4
Putative uncharacterized protein	Q580M1	4
Dihydrolipoamide acetyltransferase, putative	Q38AK7	3.6
73 kDa paraflagellar rod protein	Q580L2	3.1
Putative uncharacterized protein	Q380Y7	3.1
Tricarboxylate carrier, putative	Q38FB0	3.05
Mitochondrial processing peptidase alpha subunit	Q386B6	3
Alanine aminotransferase, putative	Q4GYI2	3

only TbTim17 was *in situ* tagged with 6xMyc and observed that 6xMyc-TbTim17 is localized in mitochondria. VDAC and TbPP5 were used as the mitochondrial and cytosolic marker
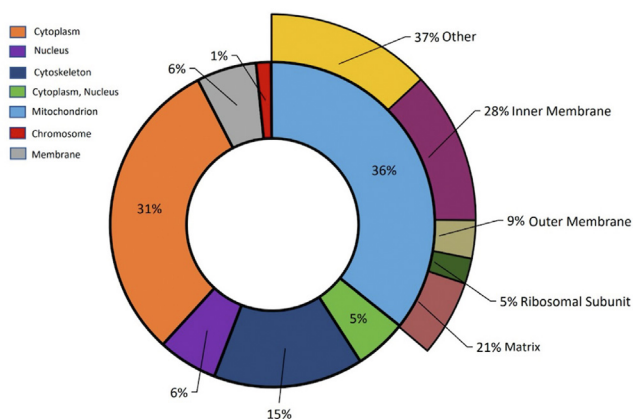

Figure 4. Analysis of the mass-spectrometry results. Data files produced from duplicate sets of MS-MS were parsed into Scaffold (version 5.0.1) for filtering and validation. Proteins identified with high confidence and enriched 3- to 12-fold in the sample from induced BirA*-TbTim17 cells were enlisted. GO annotation was conducted for cellular component of the biotinylated proteins to identify their subcellular localization. The proteins were submitted to the UniProtKB mapping tools for annotation. The percentage of proteins with a given GO term is indicated in the corresponding slices with different colors as indicated in the key in the pie chart. In the mitochondrial protein layer of the chart, well-characterized proteins were annotated as matrix, inner membrane, outer membrane, and ribosomal subunits. Others include proteins for which submitochondrial locations were not determined. GO, Gene Ontology; MS, mass spectrometry.

proteins, respectively. In addition, we performed *in situ* immunofluorescence analyses of the doubly tagged cells using anti-Myc (rabbit polyclonal) and anti-HA (mouse monoclonal) primary antibodies. Secondary antibodies were FITC-conjugated anti-rabbit IgG and Alexa Flour–conjugated anti-mouse IgG (Fig. 5C). Merged pictures clearly showed that 6xMyc-TbTim17 and TbTRAP1-3xHA are colocalized with a Pearson's coefficient of 0.82; 4′,6-diamidino-2-phenylindole was used to stain the nuclear and mitochondrial DNAs. Phase contrast images showed the parasite morphology. These results further demonstrated that TbTRAP1 is colocalized in mitochondria with TbTim17.

Next, we performed coimmunoprecipitation analysis of 6xMyc-TbTim17 and TbTRAP1-3xHA from mitochondrial lysates using anti-Myc and anti-HA antibody-coupled agarose beads. Results showed a weak interaction of these two proteins under normal conditions (Fig. 6, A and B). Anti-Myc–coupled agarose beads pulled down 6xMyc-TbTim17 along with a small fraction of TbTRAP1-HA (Fig. 6A). Similarly, anti-HA antibody precipitated TbHSP84-3xHA completely, along with a small fraction of 6xMyc-TbTim17 (Fig. 6B). However, none of these antibodies precipitated VDAC, an abundant protein in the mitochondrial lysate. These data revealed that TbTRAP1 and TbTim17 transiently or weakly interact with each other and that TbTRAP1 is not a core component of the TbTIM17 complex. As a chaperone protein, TbTRAP1 could have more affinity for the unfolded or partially folded TbTim17. To test our hypothesis, we solubilized the mitochondrial protein with 1% SDS and then diluted 20-fold with 0.2% Triton X-100-containing buffer for renaturation before immunoprecipitation with anti-Myc or anti-HA antibody-coupled agarose beads. Surprisingly, we found that specific interaction between 6xMyc-TbTim17 and TbTRAP1-3xHA increased several folds during this denaturation/renaturation process (Fig. 6, C and D). Anti-Myc antibody precipitated a significant proportion of 6xMyc-TbTim17 and TbTRAP1-3xHA (Fig. 6C). Similarly, most of the 6xMyc-TbTim17 was precipitated with TbTRAP1-3xHA by anti-HA antibody (Fig. 6D). Probing the blots with TbHsp70, VDAC, and RBP16 antibodies demonstrated that these proteins were present only in the total and unbound fractions and not in the pellet fractions when pulled down either with anti-HA or anti-Myc. These data clearly showed that the interaction between TbTim17 and TbTRAP1 is specific under this condition. Therefore, it appears that TbTim17 is a specific client protein of TbTRAP1 in mitochondria.

TbTRAP1 knockdown hampered the integrity of the TbTIM17 complex and reduced the levels of TbTim17, TbTim62 and, mHsp70

To investigate the role of interaction between TbTim17 and TbTRAP1, we performed knockdown of TbTRAP1 by RNAi. We used the TbTRAP1-3xHA as the parental cell line to monitor the levels of the target proteins. Expression of the dsRNA for TbTRAP1 from an inducible expression vector reduced cell growth significantly (Fig. 7A), revealing that
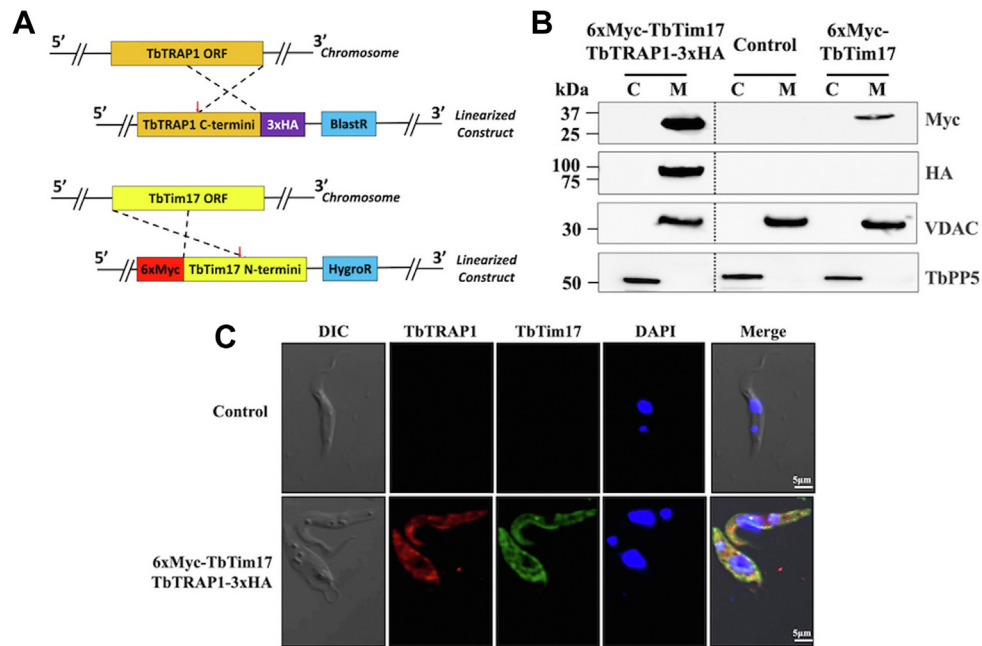
Figure 5. Expression and subcellular localization of *in situ* tagged TbTRAP1-3xHA and 6XMyc-TbTim17 in *T. brucei*. *A*, schematics of the *in situ* tagging strategy. Targeting loci of TbTRAP1 and TbTIM17 in chromosomes are shown. Under each targeting locus, the corresponding *in situ* tag constructs are depicted. Crossovers for homologous recombination are shown by *dashed lines*. *Red arrows* indicate the linearization sites in the construct. *B*, mid-log phase *T. brucei* expressed both 6xMyc-TbTim17 and TbTRAP1-3xHA, only 6xMyc-TbTim17, and the parental control cells were harvested. The cytosolic (C) and mitochondrial fractions were isolated by digitonin extraction as described in the Experimental procedures. Proteins from these fractions were separated on SDS-PAGE, transferred to nitrocellulose membrane, and probed with antibodies for Myc and HA epitopes. VDAC and TbPP5 were used as mitochondrial and cytosolic markers. *C*, *in situ* immunofluorescence analysis of *T. brucei* procyclic form expressed both TbTRAP1-3xHA and 6xMyc-TbTim17. The parental Pro427 cells were used in parallel as control. Anti-Myc polyclonal (rabbit) and anti-HA monoclonal (mouse) were used as primary antibodies, and anti-rabbit IgG conjugated with FITC and antimouse IgG-coupled Alexa Flour were used as secondary antibodies, respectively. DAPI was used to stain the nuclear and mitochondrial DNAs and merged images are shown. Phase construct images (DIC) are presented. Scale bars are indicated. DAPI, 4′,6-diamidino-2-phenylindole; HA, hemagglutinin; VDAC, voltage-dependent anion channel.

TbTRAP1 is required for cell proliferation. A recent report shows that TbTRAP1 knockdown inhibits cell growth of the *T. brucei* bloodstream form (33); therefore, TbTRAP1 is essential for both forms of *T. brucei*. Next, we performed BN-PAGE analysis to investigate the effect of TbTRAP1 knockdown on the TbTIM17 complex (Fig. 7B). Immunoblot analysis after separation of mitochondrial protein complexes from uninduced and induced cells using BN-PAGE with anti-HA antibody showed a strong band of the monomeric TbTRAP1 (84 kDa) in the uninduced sample. In addition, the dimeric and other multimeric forms of TbTRAP1 were present (Fig. 7B). It has been reported in the mammalian system that unlike cytosolic Hsp90, TRAP1 does not require any cochaperones and works as dimeric and tetrameric forms (39). Therefore, our results suggest that this also is true for TbTRAP1 in *T. brucei*. Knockdown of TbTRAP1 by RNAi reduced the levels of all monomeric and multimeric forms of this protein, indicating that these are indeed complexes formed by TbTRAP1. Probing the blot with TbTim17 antibody revealed that in the uninduced sample TbTIM17 complexes were present within the range of 300 kDa to 800 kDa, as reported previously (Fig. 7B). However, these complexes were significantly reduced in the induced sample for TbTRAP1 RNAi. We also probed our blot with antibodies for TbTim62, a component of the TbTIM17 complex. On BN-PAGE, TbTim62 is primarily found as a ~150 kDa and a smaller

fraction is present in larger (~800 kDa) complexes (30). All these complexes significantly reduced in TbTRAP1 knockdown sample. In contrast, we did not observe any reduction of the VDAC complexes in the induced *versus* uninduced samples (Fig. 7B). Similarly, ATP synthase complex were minimally affected (Fig. 7B). Next, we probed our blot with Atom69 antibody to check the effect of TbTRAP1 knockdown on Atoms. Previous report showed that unlike other Atom subunits, Atom69 is found in two different size complexes (>669 kDa and ~150 kDa) on BN-PAGE (21). We also noticed similar pattern of protein complexes with anti-Atom69 antibody. TbTRAP1 knockdown minimally reduced the lower molecular size complex; however, the larger complex levels were unaltered. Interestingly, we observed a major change in the protein complexes consisting of mitochondrial HSP70 (mHsp70). In the uninduced sample, mHsp70 was present in multiple complexes within the range of 400 to >880 kDa. mHsp70 has many client proteins and it is associated with different cochaperones. Therefore, it is likely that mHsp70 could be present in different size complexes in mitochondria. TbTRAP1 knockdown abolishes two out of three such complexes seen on BN-PAGE. This result suggests that these two chaperone proteins, mHsp70 and TbTRAP1, interact and work together in protein folding and assembly processes, as reported in other systems (39–41). Coomassie blue–stained BN-PAGE gel showed that proteins were loaded equally from the
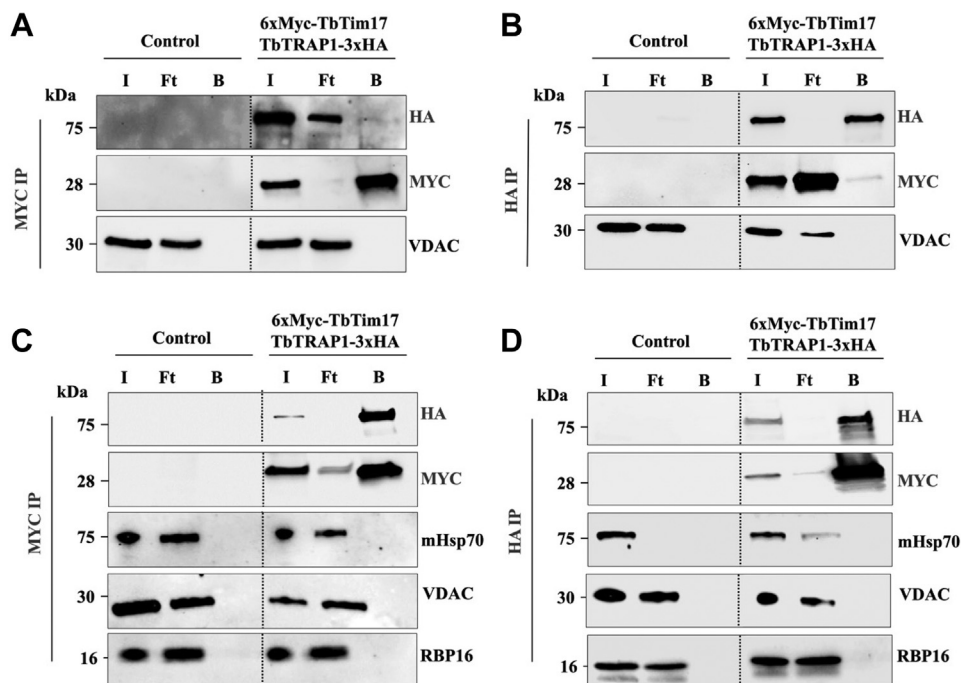
Figure 6. Coimmunoprecipitation analysis of TbTim17 and TbTRAP1 from *T. brucei* mitochondrial lysate. *A* and *B*, mitochondrial proteins from *T. brucei* expressing both 6xMyc-TbTim17 and TbTRAP1-3xHA were solubilized with digitonin (1.0%) and subjected for immunoprecipitation with anti-Myc (*A*) and anti-HA (*B*) antibody-coupled agarose beads. Mitochondrial lysate from the parental control cells was used in parallel. Input (I), flowthrough (Ft), and bound (B) proteins were analyzed by immunoblot analyses probing with HA, Myc, and VDAC antibodies. *C* and *D*, mitochondrial proteins from *T. brucei* expressing both 6xMyc-TbTim17 and TbTRAP1-3xHA were solubilized first with 1% SDS and diluted 20-fold with buffer containing 0.2% Triton X-100, as described in the Experimental procedures section. Solubilized proteins were subjected for immunoprecipitation with anti-Myc (*C*) and anti-HA (*D*) antibody-coupled agarose beads. Input (I), flowthrough (Ft), and bound (B) proteins were analyzed by immunoblot analysis probing with HA, Myc, mHsp70, VDAC, and RBP16 antibodies. HA, hemagglutinin; VDAC, voltage-dependent anion channel.

uninduced and induced samples. To analyze the effect of TbTRAP1 on TbTIM17 complex, we also performed two-dimensional BN-SDS-PAGE analysis of mitochondrial proteins (Fig. S3). Gel strips from the first dimension BN-PAGE for TbTRAP1 RNAi induced and uninduced mitochondria samples were run on a denaturing gel in second dimension, transferred to the nitrocellulose membrane, and sequentially probed with antibodies for HA-epitope (TbTRAP1-3HA), TbTim17, and VDAC. Results further confirmed that the levels of TbTRAP1-3HA were significantly reduced in the induced mitochondria in comparison to the uninduced control. TbTim17 protein was strongly detected in the region of the second-dimension gel corresponding to the location of 300 to >800 kDa in the first dimension from uninduced sample; however, very little protein was detected at the corresponding region of the BN-PAGE blot for the induced sample. VDAC was detected similarly from both samples, as expected. These results clearly showed TbTim17 was not assembled in the higher molecular mass complex, when TbTRAP1 levels were reduced by RNAi.

Next, we investigated the effect of TbTRAP1 knockdown on the steady-state levels of different mitochondrial proteins (Fig. 7C). As expected, TbTRAP1-3xHA levels were below the detection limit in the induced sample. TbTim17 and TbTim62 levels were reduced about 40% and 60%, respectively, due to knockdown of TbTRAP1 (Fig. 7, *C* and *D*). In contrast, the levels of Atom69 and TbATPase β subunit were reduced 5%

and 20%, respectively. Levels of RBP16, a mitochondrial matrix protein, reduced 10% to 12%. Whereas, the steady-state level of mHsp70 reduced about 30% (Fig. 7, *C* and *D*). These results strongly correlated with data obtained from BN-PAGE analysis. Together, it showed that TbTRAP1 knockdown hampered the assembly of the TbTIM17 complex, and consequently, the levels of the core components TbTim62, mHsp70, and TbTim17 were reduced.

To obtain a global view of TbTRAP1 depletion on the mitochondrial proteome, we performed semiquantitative proteomics analysis. Multidimensional protein identification (MudPIT) MS of the triplicate mitochondria samples from TbTRAP1 RNAi induced and uninduced cells and statistical analysis for significance, we found the levels of 42 different proteins were altered within the range of 0.03- to 16-folds (Table S2). Among these, TbTRAP1 was the most down-regulated protein, as expected (Fig. 7E). We also found TbTim62 in the significantly downregulated proteins, which supports our BN-PAGE and SDS-PAGE results. Among other downregulated proteins we found Atom14, an ATOM subunit (43). Unlike Atom69, which is a receptor subunit and mostly exposed in the cytosolic side, Atom14 is a core component of the ATOM complex. It is possible that the effect of the TbTIM17 complex due to TbTRAP1 knockdown have spread on the core part of the ATOM complex, since TbTIM17 and ATOM are closely positioned at least during translocation of proteins. Additionally, the kineto-flagellar zone proteins, like
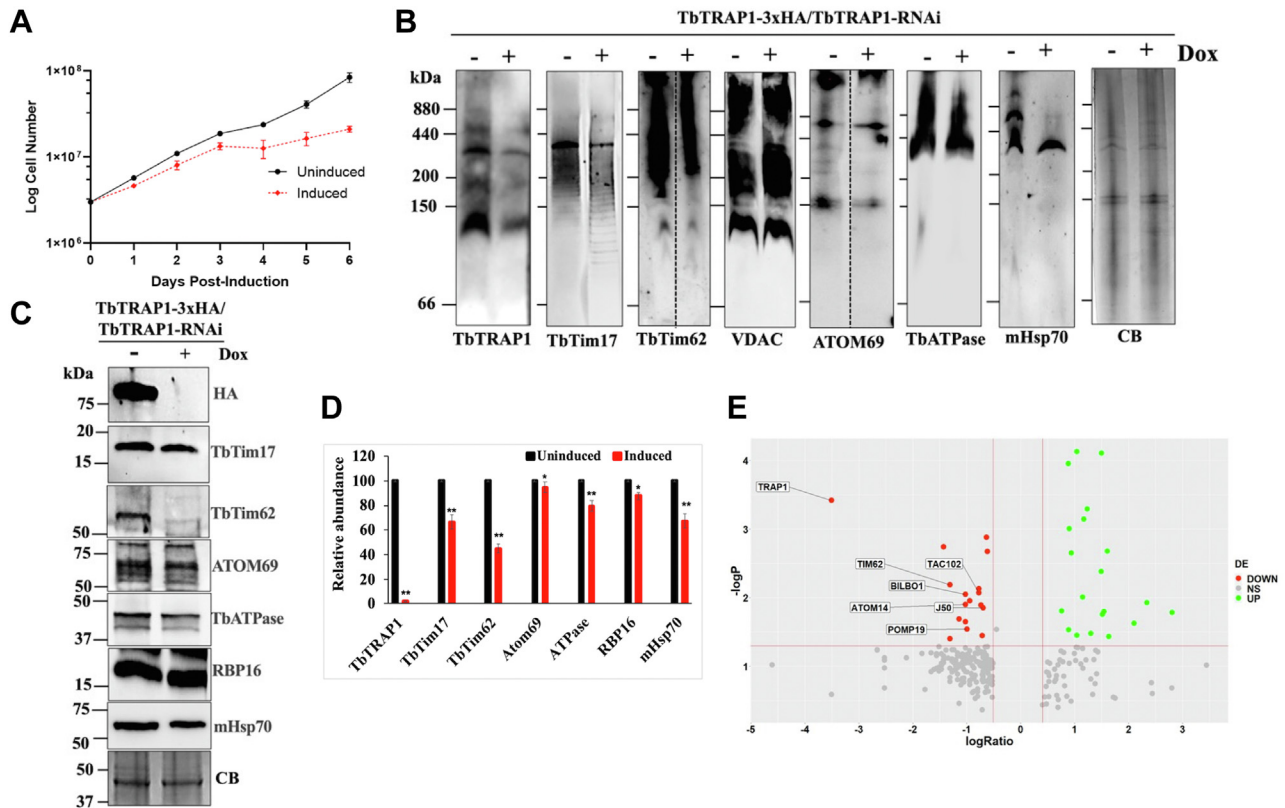
Figure 7. Effect of TbTRAP1 RNAi on TbTIM17 protein complex. *A*, TbTRAP1 RNAi cells were grown in the presence and absence of doxycycline for induction of TbTRAP1 dsRNA expression. Cell numbers were counted daily for 6 days, and a log of cumulative cell numbers was plotted *versus* time post-induction. *B*, BN-PAGE analyses of mitochondrial protein complexes. *T. brucei* cells expressed *in situ* tagged TbTRAP1-3xHA and tetracycline-inducible TbTRAP1 dsRNA (TbTRAP1-3xHA/TbTRAP1-RNAi) were grown for 2 days in the absence (−) and presence (+) of doxycycline for isolation of mitochondria. Mitochondrial proteins were solubilized with 1% digitonin and subjected to BN-PAGE, followed by immunoblot analyses using HA (TbTRAP1), TbTim17, VDAC, mHsp70, Atom69, and TbATPase antibodies for detection of the respective complexes. Coomassie blue (CB)–stained gel image are shown as the loading control. *C*, TbTRAP1-3xHA/TbTRAP1-RNAi cells were grown for 2 days in the absence (−) and presence (+) of doxycycline for isolation of mitochondria. Total mitochondrial proteins were analyzed by immunoblot analyses using antibodies for HA, TbTim17, TbTim62, RBP16, and Atom69. *D*, quantitation of the levels TbTRAP1-3xHA, TbTim17, TbTim62, Atom69, ATPase β, RBP16, and mHsp70 in TbTRAP1-RNAi induced cells relative to uninduced control. Experiments were conducted three times, and significance values were calculated by *t* test and indicated by asterisks as follows: **$p < 0.01$ and *$p < 0.05$. *E*, volcano plot with protein enrichment detected by mass spectrometric label-free quantitation. Differences in protein enrichment between control and experimental samples was evaluated with a Student's *t* test across three biological replicates. The horizontal axis indicates log 10 ratio of protein abundance of experimental to control groups. The vertical axis shows -log 10 of the *t* test *p*-value. Upregulated proteins are shown in *green*, downregulated proteins are shown in *red*, and nonsignificant proteins are shown in *gray*. Proteins with statistically significant differential expression ($p < 0.05$) are located above the *red* horizontal line (*p* value = 0 0.05) and the *red* vertical lines denote a ratio of log 10 ±1.5. BN, blue-native; HA, hemagglutinin; VDAC, voltage-dependent anion channel.

TAC102 (44) and a flagellar pocket collar protein, BILBO1 (45) were reduced (Fig. 7*E*), which could explain the defective kinetoplast DNA (kDNA) replication caused by depletion of TbTRAP1, as reported earlier (33). Some metabolic enzymes related to nucleotide biosynthesis and pentose phosphate pathway, like adenylosuccinate synthetase and ribose-5-phosphate isomerase, respectively, were upregulated (Table S2), likely due to energy crisis for all these changes.

TbTRAP1 knockdown reduced the assembly of the newly synthesized TbTim17 into the TbTIM complex

To understand the role of TbTRAP1 on TbTIM17 complex assembly, we expressed TbTim17-2xMyc from an inducible expression vector in TbTRAP1-3xHA/TbTRAP1-RNAi cells (Fig. 8). The constructs for developing this cell line are shown in Figure 8*A*. These cells upon induction with doxycycline expressed TbTim17-2xMyc and the dsRNA for TbTRAP1,

simultaneously. *T. brucei* cells that produce only TbTim17-2xMyc after induction with doxycycline were used as the control. Immunoblot analysis of the mitochondrial fractions isolated from TbTim17-2xMyc cells induced and TbTRAP1-3xHA/RNAi/TbTim17-2xMyc cells uninduced and induced with doxycycline were performed to compare the levels of TbTim17-2xMyc and TbTRAP1-3xHA. As expected, TbTRAP1-3xHA levels were reduced about 90% due to induction of RNAi (Fig. 8*B*). The TbTim17-2xMyc (control) cells do not have the *in situ* tagged TbTRAP-3xHA, thus no protein was detected by anti-HA antibody from this sample. TbTim17 antibody detected both the endogenous TbTim17 and the ectopically expressed TbTim17-2xMyc. Anti-myc antibody only recognized the ectopic copy from the induced samples and not from the uninduced TbTRAP1-3xHA/RNAi/TbTim17-2xMyc sample. The levels of the TbTim17-2xMyc in the control and TbTRAP1 RNAi mitochondria samples were comparable, indicating that TRAP1 depletion did not

hamper the import of the newly synthesized TbTim17-2xMyc into mitochondria. Atom69, RBP16, and VDAC levels were similar in all samples. Next, we performed BN-PAGE analysis to investigate if TbTRAP1 depletion has any effect on the assembly of TbTim17-2xMyc in the TbTIM complex (Fig. 8*C*). We found that TbTim17-2xMyc assembled into the higher molecular mass (300–800 kDa) complexes in the induced TbTim17-2xMyc mitochondria, as we reported earlier (30). However, the assembly of TbTim17-2xMyc into such complexes was significantly reduced when TbTRAP1 was depleted. We have seen a protein band near 800 kDa in this sample; however, a similar size band is also present in the uninduced sample, suggesting this is at least partly due to nonspecific interaction of Myc antibody. A similar nonspecific band with this antibody has been shown in our previous report (30). Probing the blot with TbTim17 antibody showed that the levels of the TbTim17 complexes were comparable in the uninduced TbTRAP1-3xHA/RNAi/TbTim17-2xMyc sample

and induced control (TbTim17-2xMyc). However, TbTim17 complex levels were reduced in the induced TbTRAP1-3xHA/ RNAi/TbTim17-2xMyc sample as expected. Coomassie-stained gel was used to show protein loading. These experiments clearly showed that TbTRAP1 is required for the formation of the TbTIM17 complexes.

Overall, we found TbTRAP1 is essential for growth of the *T. brucei* procyclic form. We have also elucidated an important function of TbTRAP1 in *T. brucei* mitochondrion. We found that TbTRAP1 interacts with TbTim17 and depletion of TbTRAP1 significantly reduced the levels of TbTIM17 complex as well as the levels of multiple subunits of this complex. Finally, we showed that TbTRAP1 depletion hampered the assembly of TbTim17-2xMyc into the TbTIM complex. Thus, it appears that TbTRAP1 is an important assembly factor for the TbTIM17 in *T. brucei*. Here, we proposed a model for TbTIM complex biogenesis in mitochondria (Fig. 9). TbTim17 is a nucleus-encoded protein; therefore, it requires to be
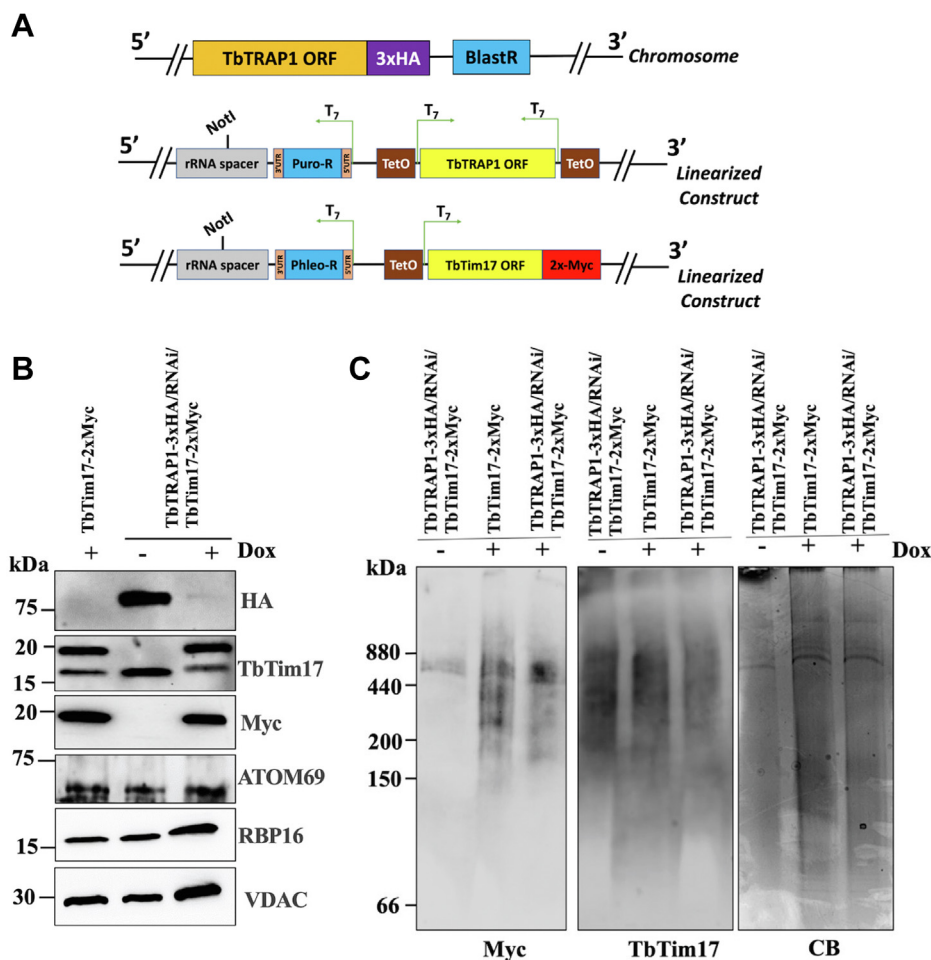

Figure 8. Assembly of TbTim17-2xMyc into the TbTIM complex in TbTRP1-depleted *T. brucei*. *T. brucei* cells express TbTim17-2xMyc alone and with TbTRAP1 dsRNAs in the background of *in situ* tagged TbTRAP1-3xHA upon induction with doxycycline were used to analyze the import and assembly of the TbTim17-2xMyc. *A*, schematics for the *in situ* tagged TbTRAP1-3xHA in the *T. brucei* genome and the constructs for the expression of TbTim17-2xMyc and TbTRAP1 dsRNA. Tetracycline operator (TetO) and the direction of transcription by T7 polymerase are shown. *B*, immunoblot analysis of the mitochondrial proteins from the TbTRAP1-3xHA/TbTRAP1-RNAi/TbTim17-2xMyc cells uninduced (-) and induced for 4 days with doxycycline were probed with different antibodies as indicated. Mitochondrial proteins from TbTim17-2xMyc cells induced for the same time were analyzed in parallel as the control. *C*, BN-PAGE analysis of the mitochondrial proteins from the TbTRAP1-3xHA/TbTRAP1-RNAi/TbTim17-2xMyc uninduced (−) and induced (+) for 4 days with doxycycline were probed with anti-myc and Anti-TbTim17 antibodies. Mitochondrial proteins from the TbTim17-2xMyc cells, induced for the same time, were analyzed in parallel as the control. CB represents the image of the Coomassie-stained gel. BN, blue-native.

imported into mitochondria from cytosol and assembled in the MIM. We observed that BirA*-TbTim17 biotinylates Atom46 and Atom69, the two receptor-translocases of the ATOM complex, suggesting TbTim17 may require both receptors for its import (Fig. 9). TbTIM17 is the single translocase of the mitochondrial inner membrane in *T. brucei*, thus TbTim17 protein is imported into the inner membrane through the TbTIM17 complex. Once entered the inner membrane, TbTim17 requires to be assembled with the other components of the TbTIM17 complex. In our previous reports, we showed that TbTim62, a component of the TbTIM17 complex, is required for the assembly of the TbTIM17 and for association of TbTim17 with mHsp70 (30). Here, we observed that depletion of TbTRAP1 reduced the level of TbTim62, TbTim17, and mHsp70 significantly and hampered the assembly of the TbTIM17 complex (Fig. 8). Together, we propose that the assembly of the TbTim17 and TbTim62 with the help of the TbTRAP1 and mHsp70 is crucial for formation of the matured complex. TbTRAP1 plays an important role in this assembly process. Therefore, depletion of TbTRAP1 severely hampers this process, thus the larger complexes of TbTIM17 are not formed.

Discussion

Hsp90 homologs are widely present in both eukaryotes and prokaryotes. In eukaryotes, it is present in multiple subcellular compartments. In mitochondria, the Hsp90 homolog is known as TRAP1/Hsp84. In prokaryotes, it is named as HtpG1, which is localized in the cytoplasm (41). Mitochondrial Hsp84 or TRAP1 is a known cancer target and has been studied mostly in mammalian systems (34–36). Roles of TRAP1 in regulation of cellular bioenergetics and mitochondria-mediated cell

apoptosis have been documented (37–39, 46). However, TRAP1 interactions with the mitochondrial protein translocases have not been studied. Furthermore, the function of TRAP1 in the mitochondria in unicellular eukaryotes mostly remains unexplored. Here, we demonstrated for the first time that TbTim17 indeed interacts with TbTRAP1 in the procyclic form of *T. brucei*. In addition, we demonstrated that TbTRAP1 is needed for folding/assembly of TbTim17 to form the TbTIM complex, the single translocase of the mitochondrial inner membrane in *T. brucei*.

BioID is a powerful tool to identify proximal proteins even when these are transiently associated with the bait protein. BioID has been used successfully to identify novel interactors of the flagellar basal body (45, 47), other cytoskeleton structures (48), and RNA-binding proteins (49) in *T. brucei*. Here, we used this approach to characterize the TbTim17 interactome in this parasite. The central part of the TbTim17 protein is mostly membrane integrated; however, its N- and C-terminals are hydrophilic (23). We found the N-terminally BirA*-tagged TbTim17 was expressed and targeted to mitochondrial membrane. Based on our results that BirA*-TbTim17 was present in a higher molecular mass protein complex, similar in size to that of TbTIM17, and it was coimmunoprecipitated with the endogenous TbTim17; we conclude that BirA*-TbTim17 was assembled in the TbTIM17 complex at least in part. Therefore, it may be expected that any proteins encountering BirA*-TbTim17 during this process could be biotinylated, provided the lysine residue(s) of the prey proteins are within 10 nm distance from the BirA* catalytic domain. It is also conceivable that as BirA*-TbTim17 is present in the complex, some substrate proteins could be biotinylated during their import. For these reasons, we found that a wide variety of mitochondrial proteins were biotinylated by
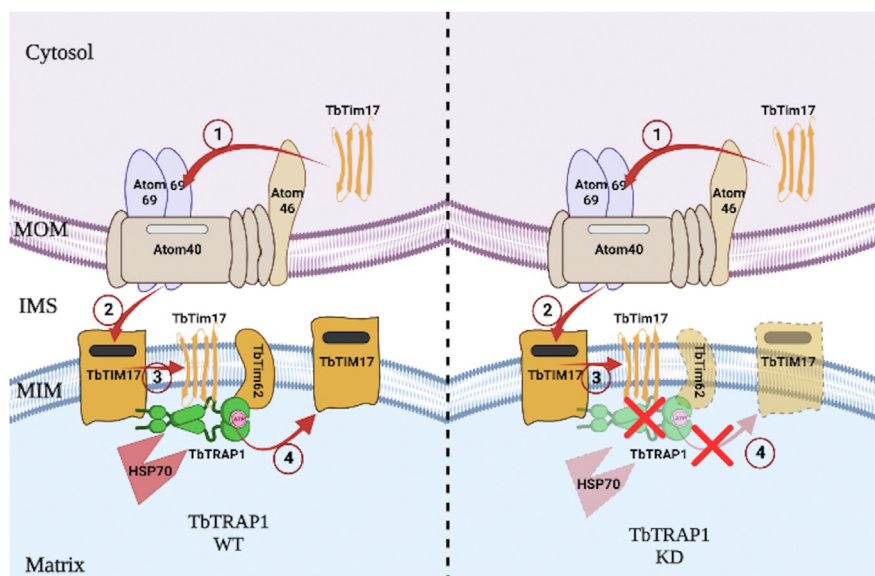

Figure 9. A schematic of the role of TbTRAP1 on TbTIM17 complex biogenesis. The simplified form of the mitochondrial outer and inner membrane translocases, ATOM and TbTIM17, respectively, are shown. The translocation pathway of TbTim17, a nuclear-encoded mitochondrial protein, is indicated by *red arrows*. The left panel represent the translocation of TbTim17 and its assembly in the TbTIM17 complex in the inner membrane in the WT parasite. Whereas, the right panel shows the pathway that is hampered due to depletion of TbTRAP1 (TbTRAP1 KD). Abbreviations used are MOM; mitochondrial outer membrane, MIM; mitochondrial inner membrane, IMS; intermembrane space. TbTim17 represents the protein TbTim17, TbTIM17 represents the TbTim17 complex. TbTRAP1 shown as homodimer.

BirA*-TbTim17. Among the previously identified ATOM and TbTIM subunits, we found Atom46, Atom69, and TbTim17 were biotinylated. It is possible that Atom46 and Atom69, two receptor subunits of the ATOM complex, are required for import of TbTim17 into mitochondria. As reported previously, these two ATOM subunits also were copurified during tandem affinity purification of TbTim17 while it was tagged at the C-terminal with a tandem affinity purification tag (20). Therefore, it is likely that the hydrophilic termini of TbTim17 somehow are in close association with these receptors, particularly when ATOM and TbTIM are in close contact during mitochondrial protein import; however, it requires further investigation to verify this assumption. In contrast to the ATOM subunits, previously identified TbTims, including TbTim62, TbTim42, TbTim54, and others, were not enriched in the streptavidin pull-down fraction. This suggests that in the assembled complex, either these TbTims are not in close association with the TbTim17 termini or the lysine residues in these proteins are not exposed and/or in position to be biotinylated. We found several other proteins like GST/gluta-redoxin and minicircle binding protein, among the enriched biotinylated proteins by BirA*-TbTim17; however, the significance of these is not clear at this moment.

Interestingly, TbTRAP1 was found to be highly enriched biotinylated proteins by BirA*-TbTim17. TbTRAP1 could be present in the matrix or in the IMS in mitochondria. However, no report of interaction of these two proteins in mitochondria has been made previously. Therefore, we chose this prey protein for further validation. As in Hsp90 family proteins, TRAP1 has three structural domains (1): the N-terminal domain is responsible for ATP binding and hydrolysis (2); the middle portion is the substrate-binding domain; and (3) the C-terminal domain is responsible for dimerization. TRAP1 exists as a homodimeric or homotetrameric (dimer of a dimer) forms to function as a chaperone (39). BN-PAGE analysis of the *in situ* tagged TbTRAP1 also revealed the presence of dimeric and tetrameric forms under native conditions, suggesting TbTRAP1 functions as a chaperone in mitochondria in *T. brucei*. As with other chaperones, TRAP1 transiently interacts with its client proteins. We also observed that a small fraction of TbTRAP1 coprecipitated with TbTim17 under normal conditions, suggesting a weak, but specific, interaction between these two proteins. However, we found a much larger fraction of TbRAP1 was coprecipitated with TbTim17 when mitochondrial proteins were first denatured with SDS and then renatured by dilution with a nonionic detergent. This suggests that TbTRAP1 is needed for refolding of TbTim17, and this is specific, as we did not observe similar results for other mitochondrial proteins.

In addition, depletion of TbTRAP1 significantly reduced the levels of the assembled TbTIM17 complex. Some of the complexes of the mHsp70 were also significantly altered. However, other major complexes in the mitochondrial inner and outer membranes, like ATP-synthase and VDAC, respectively, were not affected due to depletion of TbTRAP1, showing the specific requirement of TbTRAP1 for TbTIM17 assembly/integrity. Furthermore, TbTRAP1 reduction significantly reduced the levels of TbTim62, a core component of the TbTIM17 complex. In our previous reports, we showed that TbTim62 is present in a ~150 kDa, as well as in higher molecular mass complexes, coprecipitated with TbTim17 and is required for association of TbTim17 with mHsp70, a part of the import complex (30). Together, it suggests that TbTRAP1 may facilitate the association of TbTim17, TbTim62, and mHsp70, which is required for the formation of the larger TbTIM17 complexes. TbTRAP1 depletion hampered this association, consequently, the assembly of the larger complexes of TbTIM17 hindered. We further showed that the ectopically expressed TbTim17-2xMyc were accumulated in the mitochondria in TbTRAP1 depleted *T. brucei*, suggesting that the import and stability of TbTim17 do not require this chaperone protein. However, we found that TbTRAP1 is critical for the following step that is the assembly of the imported protein with other subunits to form the functional complex. Overall, we showed that TbTRAP1 acts as a chaperone for the assembly of the TbTim17 complex in *T. brucei* procyclic form.

It has been reported recently that TbTRAP1 is essential for replication of the mitochondrial DNA (kDNA) in the bloodstream form of *T. brucei* that dwells in mammalian systems (33). As all proteins needed for kDNA replication are nuclear DNA encoded and presumably are imported through the TbTIM complex, it is conceivable that disruption of this complex due to depletion of TbTRAP1 could affect the kDNA replication. However, we also cannot exclude the possibility that TbTRAP1 directly interacts with the replication proteins. In this report, we found that depletion of TbTRAP1 reduced the levels of the tripartite attachment (TAC) complex subunit, TAC102, which is positioned very close to the kDNA (44). TAC102 is required for kDNA segregation and maintenance. Therefore, reduction of TAC102 due to TbTRAP1 knockdown could be connected to the observed effect on kDNA replication defect. In any case, it is now confirmed that TbTRAP1 is essential for mitochondrial functions in both the procyclic and bloodstream forms of *T. brucei*.

Overall, our studies elucidate a novel function of TRAP1 in mitochondria that has not been reported previously in any system. It has been reported in the mammalian system that TRAP1 not only regulates mitochondrial bioenergetics by interacting with succinate dehydrogenase and cytochrome oxidase complexes but also interacts with cyclophilin D and regulates mitochondrial permeability transition pore opening for induction of apoptosis (35, 36, 46). A recent interactome study identified several other mitochondrial proteins including Tim50 and Tim23; however, these results were not experimentally verified and functional consequences have not been tested. Here, we showed that TbTRAP1 is a valid interactor of TbTim17 in *T. brucei* and plays a crucial role in the assembly of the TIM complex in this parasitic protozoan. Therefore, this knowledge could be corroborated for the TIM complexes in other eukaryotes. Furthermore, trypanosomatid possesses a single TIM complex that imports various proteins as well as tRNAs (8). Therefore, it can be assumed that a dynamic association and dissociation of various subunits of the TbTIM17 complex is necessary to operate these functions. In this

respect, the association of TRAP1 with the TbTIM17 complex could be more meaningful. Future studies will elucidate more mechanistic process of this interaction during mitochondrial protein import.

Experimental procedures

Cell maintenance, growth medium, and cell growth analysis

The procyclic form of the *T. brucei* 427 doubly resistant cell line (29–13), expressing a tetracycline repressor gene and a T7 RNA polymerase was grown in SDM-79 medium supplemented with 10% fetal bovine serum, G418 (15 µg/ml), and hygromycin (50 µg/ml). To measure growth, cells were seeded at a density of 2×10^6 cells/ml in fresh medium containing the appropriate antibiotics. For induction of RNAi or over-expression, doxycycline (1.0 µg/ml to 1.5 µg/ml) was added in the medium. At different time points after induction, cell number was counted using a Neubauer hemocytometer. The log of cumulative cell numbers was plotted *versus* time (in days) of incubation.

Generation of plasmid constructs and **T. brucei** *transgenic cell lines*

For generation of BirA*-TbTim17, expression constructs, the ORF of TbTim17 (Tb927.11.13290) was subjected to PCR amplification using *T. brucei* 427 genomic DNA as the template and the corresponding sequence-specific primers (Table S1). The forward and reverse primers were designed to add restriction sites for XhoI and BamHI at the 5′ and 3′ ends of the ORF, respectively. The PCR products were cloned into the pLew100-Myc-BirA* vector within XhoI and BamHI restriction sites (45). Plasmid DNA was linearized by NotI digestion and transfected into *T. brucei* 29-13 cells, as previously described (27). Transfected cells were selected with phleomycin (2.5 µg/ml). The TbTRAP1 RNAi construct was generated by PCR amplification of the region 253 bp to 758 bp in the ORF of TbTRAP1 (Tb927.11.2650) using *T. brucei* genomic DNA as the template and sequence-specific primers (Table S1). The forward and reverse primers were designed to add restriction sites for HindIII and BamHI at the 5′ and 3′ ends of the ORF, respectively. The PCR product was cloned into a tetracycline-inducible T7 double-headed promoter p2T7^{Ti}-177 RNAi vector between the HindIII and BamHI restriction sites (50). Plasmid DNA was linearized by NotI digestion and transfected into *T. brucei* 29-13 cells. Transfected cells were selected with puromycin (1.0 µg/ml). The TbTRAP1 RNAi puromycin-resistant cells then were transfected with the *in situ* tagging construct of TbTRAP1-3xHA generated using pNAT vector. *In situ* epitope tagging of one of the two loci of the TbTRAP1 construct was created using the pNAT-12MYC vector (51). Briefly, the synthetic C-terminal coding fragment (1354 bp to 2241 bp) of TbTRAP1 ORF (C/TbTRAP1), excluding the stop codon, but containing three HA epitopes with a stop codon at the 3′-end, was cloned into the pNAT vector in between AscI and BamHI sites. The pNAT-C/TbTRAP1 construct was linearized by CsiI digestion and transfected into the TbTRAP1 RNAi cell line. Transfected

cells were selected with blasticidin (10.0 µg/ml). The *T. brucei* 427 cell line also was transfected with the pNAT-C/TbTRAP1 construct. Furthermore, the *T. brucei* 427 cell line expressing TbTRAP1-3xHA was transfected with the pNAT-6xMyc-TbTim17 construct to generate doubly expressed 6xMyc-N/TbTim17 and TbTRAP1-3xHA. For generation of the pNAT-6xMyc-TbTim17 construct, the N-terminal coding fragment (1 bp to 285 bp) of TbTim17 ORF was amplified by using forward and reverse primers (Table S1) and cloned into the pNAT-6xMyc vector in between AvrII and BamHI sites. The resulting construct was digested with SnaBI and used to transfect 427 procyclic form cells, as well as the newly generated TbTRAP1-3xHA. The transformed cells were selected with hygromycin (50 µg/ml). TbTim17-2xTim17 cell line was previously generated (30). The inducible expression construct in pLew100 for TbTim17-2xMyc were used to transfect TbTRAP1-3xHA/TbTRAP1 RNAi cells to generate TbTRAP1-3xHA/TbTRAP1 RNAi/TbTim17-2xMyc cell line.

Digitonin extraction

Procyclic cells (2×10^8) were resuspended in 500 µl of SMEP buffer (250 mM sucrose, 20 mM Mops-KOH [pH 7.4], 2 mM EDTA, 1 mM PMSF) containing 0.03% digitonin and incubated on ice for 5 min. The cell suspension was then centrifuged for 5 min at 6800*g* at 4 °C. The resultant pellet was considered the crude mitochondrial fraction, and the supernatant contained soluble cytosolic proteins.

Isolation of mitochondria

Mitochondria were isolated from the parasite after lysis by nitrogen cavitation in isotonic buffer (20). The isolated mitochondria were stored at a protein concentration of 10 mg/ml in SME buffer containing 50% glycerol at −70 °C. Before use, mitochondria were washed twice with nine volumes of SME buffer to remove glycerol (20).

Alkali extraction

For sodium carbonate extraction, mitochondria (100 µg) were incubated with 100 µl of 100 mM sodium carbonate (pH 11.5) on ice for 30 min. The lysate was centrifuged at 14,000*g*, and the supernatant and pellet fractions were collected for further analysis.

SDS-PAGE and immunoblot analysis

Protein concentrations of isolated mitochondria and total cell extracts were measured using the Bradford reagent; equal amounts of proteins from different samples were resolved on SDS-PAGE gels and then transferred to nitrocellulose membranes (Bio-Rad). Antibodies against TAO (52), Hsp70 (53), TbTim17 (54), TbPP5 (55), and VDAC (56) were used as probes. The polyclonal antibodies for Atom69 peptide (CTRGLQHFEQQEIQP) were custom synthesized by Bethyl Laboratories. BirA*, HA, and Myc antibodies were purchased from Cell Signaling Technologies, Thermo Fisher Scientific, and Abcam, respectively. The secondary antibodies used were either anti-rabbit or antimouse immunoglobulins linked to

HRP (Sigma–Aldrich and Thermo Fisher). The antigens were visualized using the West Pico chemiluminescent substrate (Thermo Fisher).

Proximity-dependent protein biotinylation and purification of the biotinylated proteins

BirA*-TbTim17 *T. brucei* cells were cultivated in the absence and presence of biotin (up to 50 μM) for 12 h after growing in the presence and absence of doxycycline for 12 h. WT 29-13 cells were grown in parallel as negative control. Cells were harvest by centrifugation at 5000*g* for 10 min. Cells were washed three times with PBS and mitochondria were isolated (by digitonin extraction as previously described). Mitochondrial proteins (1 mg to 2 mg) were solubilized using 250 μl of ice-cold lysis buffer (150 mM NaCl, 20 mM Tris–HCl, pH 7.5, protease inhibitors, and 1% [vol/vol] NP-40). Next, the mixture was incubated on ice for 20 to 30 min and centrifuged at 16,000*g* for 30 min at 4 °C. The supernatant was transferred carefully to an Eppendorf tube containing 50 μl Streptavidin-coupled Dynabeads (Thermo Fisher), followed by incubation at 4 °C overnight with gentle rotation. A magnetic stand was used to separate and wash the beads five times with washing buffer (150 mM NaCl, 20 mM Tris–HCl, pH 7.5, 0.1% NP-40, and protease inhibitors). The beads were resuspended in SDS-PAGE loading buffer, and 10% of the samples were used for SDS-PAGE and immunoblot analysis. Blots were probed with HRP-conjugated streptavidin or other antibodies. The remaining 90% of the pull-down samples was analyzed by MS.

MS analysis

Prior to LC-MS analysis, equal amounts of biotinylated protein (purified by Streptavidin-conjugated beads) from the uninduced and induced BirA*-TbTim17 were denatured in 8 M urea and 50 mM Tris–HCl (pH 8.0), reduced with 10 mM Tris(2-carboxyethyl)phosphine hydrochloride for 60 min, alkylated with 2 mM iodoacetamide for 60 min, and diluted in 2 M urea with 50 mM Tris–HCl (pH 8.0) at room temperature (RT). Two micrograms of trypsin gold (Promega) were added for overnight digestion (18 h at 37 °C), and the tryptic peptides were immediately desalted using Pierce C_{18} spin columns (Thermo Fisher) at RT. Peptides were eluted with 80% acetonitrile and 0.1% formic acid and dried completely on a SpeedVac concentrator. For nano-LC-MS/MS analysis, peptides were resuspended in 5 μl of 0.5% formic acid and loaded onto a 3-phase MudPIT column (150 μm by 2 cm C_{18} resin, 150 μm by 4 cm strong cation exchange resin, filter union, and 100 μm by 12 cm C_{18} resin) as described previously (57). The digested peptides were loaded onto a HPLC column and further separated by liquid chromatography. LC-MS analyses were performed using an Eksigent AS-1 autosampler and an Eksigent nano-LC Ultra 2D pump online with an Orbitrap LTQ XL linear ion trap mass spectrometer (Thermo Finnigan) with a nanospray source. MS data acquisition was done by a data-dependent 6-event method (a survey Fourier transform mass spectrometry scan [resolution of 30,000], followed by five data-dependent ion trap scans for the five consequent most abundant ions). The general mass spectrometric settings were as follows: spray voltage of 2.4 kV, no sheath and no auxiliary gas flow, ion transfer tube temperature of 200 °C, collision-induced dissociation fragmentation (for MS/MS) with 35% normalized collision energy, activation *q* of 0.25, and activation time of 30 ms. The minimal threshold for the dependent scans was set to 1000 counts, and a dynamic exclusion list was used with the following settings: repeat count of 1, repeat duration of 30 s, exclusion list size of 500, and exclusion duration of 90 s. For protein identification and quantification, database searches were done with PEAKS 8.5 software (Bioinformatics Solution Inc.) against the forward and reverse *T. brucei* and human trypsin sequences (downloaded from GenBank). The parameters for the database search were as follows: full tryptic digestion, up to three missed cleavage sites, 20 ppm for peptide mass tolerance, 0.5 Da for fragment-mass tolerance, cysteine carbamidomethylation (+57 Da) as a fixed modification, and methionine oxidation (+16 Da) as a variable modification. Relative label-free quantification of the identified proteins was performed with the Q module of PEAKS software based on the extracted ion currents of the identified unique peptides' parent ions or a spectral counting approach, and statistically significant changes were confirmed with Fisher's exact test (*p* ≤ 0.005; Benjamini–Hochberg false discovery rate of <0.05). For MudPIT analysis of the mitochondria samples from TbTRAP1 RNAi uninduced and induced cells, equal amounts of proteins were solubilized in 2x SDS-PAGE sample buffer and run on a denaturing gel. After the proteins had penetrated 1 cm into the resolving gel, we stained the gel with Coomassie brilliant blue and excised the stained area for further analysis by trypsin digestion and MS as described previously.

Bioinformatics analysis

Data files produced from MS were parsed into Scaffold (version 5.0.1) for filtering and validation. Tables of high-confidence proteins identified by BioID for whole cell lysate and mitochondrial fraction were constructed. Scaffold thresholds were set to a peptide probability of 95% confidence and a minimum number of two peptides detected; 143 and 138 proteins met the criteria for whole cell lysate and mitochondrial fraction, respectively. Gene Ontology annotation was conducted for the cellular component of labeled proteins to identify their subcellular localization. The proteins were submitted to the UniProt Knowledgebase (UniProtKB) mapping tool (https://www.uniprot.org/mapping/). The percentage of proteins with a given Gene Ontology term was determined and represented as a piChart. Differences in protein enrichment between uninduced control and induced for TbTRAP1 RNAi samples were evaluated with a Student's *t* test across three biological replicates and represented by volcano plot.

Coimmunoprecipitation assay

Mitochondrial proteins (800 μg) were solubilized in 300 μl of 1 × cold native buffer (50 mM [Tris pH 7.2], 50 mM NaCl, 10% [wt/vol] glycerol, 1 mM PMSF, 1 μg/ml leupeptin, 1% digitonin) and incubated on ice for 1 h. The solubilized

mitochondria were centrifuged at 14,000×*g* for 30 min. An aliquot (50 μl) of the supernatant was mixed with 50 μl of 2 × Laemmli sample buffer and served as the input sample. The remaining supernatant (∼250 μl) was mixed with 25 μl of anti-Myc or anti-HA agarose bead slurry (Thermo Fisher) and allowed to incubate for 12 h at 4 °C with constant gentle inversion. The beads were then washed three times in wash buffer (50 mM Tris [pH 7.2], 50 mM NaCl, 10% [wt/vol] glycerol, 1 mM PMSF, 1 μg/ml leupeptin, 0.1% digitonin) to remove nonspecifically bound proteins. The washed beads with bound proteins were resuspended in 50 μl of 1 × Laemmli sample buffer for further analysis. For some experiments, proteins undergo an additional denaturation/renaturation step before coimmunoprecipitation analysis. Briefly, mitochondrial proteins (1 mg) were solubilized first with 100 μl buffer containing 50 mM Na-phosphate, 100 mM NaCl, 1% SDS, 1 mM PMSF, protease inhibitors, and phosphatase inhibitors for 15 to 20 min at RT. Solubilized proteins were diluted by addition of 2.0 ml of the renaturation buffer (50 mM Na-phosphate, 100 mM NaCl, 0.2% Triton X-100, protease inhibitors, and phosphatase inhibitors) and clarified by centrifugation at 100,000*g* before coimmunoprecipitation as described previously.

Immunofluorescence microscopy

Live *T. brucei* cells (5 × 10⁶) expressing TbTRAP1–3xHA and 6xMyc-TbTim17 (*in situ* tagged) were used for Mito-Tracker staining as previously described (26). Briefly, cells were washed twice with PBS and spread evenly over poly-L-lysine (100 μg/ml)–coated slides. Once the cells had settled, the slides were washed with cold PBS to remove any unattached cells. The attached cells were fixed with 3.7% paraformaldehyde and permeabilized with 0.1% Triton X-100. After blocking with 5% nonfat milk for 30 min, the slides were washed with 1× PBS. Monoclonal anti-Myc antibody and polyclonal anti-HA were used as the primary antibody; FITC-conjugated antimouse IgG and Alexa Fluor 594–conjugated anti-rabbit were used as the secondary antibodies, respectively, for visualization under a fluorescent microscope. DNA was stained with 1 μg/ml 4′,6-diamidino-2-phenylindole. Cells were imaged using a Nikon TE2000E widefield microscope equipped with a 60 × 1.4 NA Plan Apo VC oil immersion objective. Images were captured using a CoolSNAP HQ2 cooled CCD camera and the Nikon Elements Advanced Research software.

Data availability

All data are included in the article or will be available from the corresponding author M.C. Proteomics data will be submitted to TriTrypDB.

Conflict of interest—The authors declare that they have no conflicts of interest with the contents of this article.

Abbreviations—The abbreviations used are: AT, African Trypanosomiasis; BioID, Biotinylation Identification; BN, blue-native; HA, hemagglutinin; HRP, horseradish peroxidase; IMS, intermembrane space; kDNA, kinetoplast DNA; MIM, mitochondrial inner membrane; MS, mass spectrometry; MudPIT, multidimensional protein identification; VDAC, voltage-dependent anion channel.

References

1. Jensen, R. E., and Englund, P. T. (2012) Network news: the replication of kinetoplast DNA. *Annu. Rev. Microbiol.* **66**, 473–491
2. Landfear, S. M., and Zilberstein, D. (2019) Sensing what's out there - kinetoplastid parasites. *Trends Parasitol.* **35**, 274–277
3. Sternberg, J. M., and Maclean, L. (2010) A spectrum of disease in human African trypanosomiasis: the host and parasite genetics of virulence. *Parasitology* **137**, 2007–2015
4. Echavarria, N. G., Echeverria, L. E., Stewart, M., Gallego, C., and Saldarriaga, C. (2021) Chagas disease: chronic Chagas cardiomyopathy. *Curr. Probl. Cardiol.* **46**, 100507
5. Ngere, I., Gufu Boru, W., Isack, A., Muiruri, J., Obonyo, M., Matendechero, S., *et al.* (2020) Burden and risk factors of cutaneous Leishmaniasis in a peri-urban settlement in Kenya. *PLoS One* **15**, e0227697
6. Watanabe, Y., Kawaguchi, K., Saito, S., Okabe, T., Yonesu, K., Egashira, S., *et al.* (2016) An HTRF based high-throughput screening for discovering chemical compounds that inhibit the interaction between *Trypanosoma brucei* Pex5p and Pex14p. *Biochem. Biophys. Rep.* **6**, 260–265
7. Schneider, A. (2001) Unique aspects of mitochondrial biogenesis in trypanosomatids. *Int. J. Parasitol.* **31**, 1403–1415
8. Chaudhuri, M., Darden, C., Gonzalez, F. S., Singha, U. K., Quinones, L., and Tripathi, A. (2020) Tim17 updates: a comprehensive review of an ancient mitochondrial protein translocator. *Biomolecules* **10**, 1643
9. Schmidt, O., Pfanner, N., and Meisinger, C. (2010) Mitochondrial protein import: From proteomics to functional mechanisms. *Nat. Rev. Mol. Cell Biol.* **11**, 655–667
10. Bauer, M. F., Gempel, K., Reichert, A. S., Rappold, G. A., Lichtner, P., Gerbitz, K. D., *et al.* (1999) Genetic and structural characterization of the

human mitochondrial inner membrane translocase. *J. Mol. Biol.* **289**, 69–82

11. Lister, R., Hulett, J. M., Lithgow, T., and Whelan, J. (2005) Protein import into mitochondria: origins and functions today. *Mol. Membr. Biol.* **22**, 87–100

12. Schneider, A. (2020) Evolution of mitochondrial protein import - lessons from trypanosomes. *Biol. Chem.* **401**, 663–676

13. Drwesh, L., and Rapaport, D. (2020) Biogenesis pathways of alpha-helical mitochondrial outer membrane proteins. *Biol. Chem.* **401**, 677–686

14. Bauer, M. F., Sirrenberg, C., Neupert, W., and Brunner, M. (1996) Role of Tim23 as voltage sensor and presequence receptor in protein import into mitochondria. *Cell* **87**, 33–41

15. Rassow, J., Dekker, P. J. T., Van Wilpe, S., Meijer, M., and Soll, J. (1999) The preprotein translocase of the mitochondrial inner membrane: function and evolution. *J. Mol. Biol.* **286**, 105–120

16. Rehling, P., Wiedemann, N., Pfanner, N., and Truscott, K. N. (2001) The Mitochondrial import machinery for preproteins. *Crit. Rev. Biochem. Mol. Biol.* **36**, 291–336

17. Kerscher, O., Holder, J., Srinivasan, M., Leung, R. S., and Jensen, R. E. (1997) The Tim54p-Tim22p complex mediates insertion of proteins into the mitochondrial inner membrane. *J. Cell Biol.* **139**, 1663–1675

18. Koehler, C. M., Merchant, S., Oppliger, W., Schmid, K., Jarosch, E., Dolfini, L., *et al.* (1998) Tim9p, an essential partner subunit of Tim10p for the import of mitochondrial carrier proteins. *EMBO J.* **17**, 6477–6486

19. Mani, J., Meisinger, C., and Schneider, A. (2016) Peeping at Toms - diverse entry gates to mitochondria provide insights into the evolution of eukaryotes. *Mol. Biol. Evol.* **33**, 337–351

20. Singha, U. K., Hamilton, V., Duncan, M. R., Weems, E., Tripathi, M. K., and Chaudhuri, M. (2012) Protein translocase of mitochondrial inner membrane in *Trypanosoma brucei. J. Biol. Chem.* **287**, 14480–14493

21. Pusnik, M., Schmidt, O., Perry, A. J., Oeljeklaus, S., Niemann, M., Warscheid, B., *et al.* (2011) Mitochondrial preprotein translocase of trypanosomatids has a bacterial origin. *Curr. Biol.* **21**, 1738–1743

22. Rout, S., Oeljeklaus, S., Makki, A., Tachezy, J., Warscheid, B., and Schneider, A. (2021) Determinism and contingencis shaped the evolution of mitochondrial protein import. *Proc. Natl. Acad. Sci. U. S. A.* **118**, e2017774118

23. Weems, E., Singha, U. K., Hamilton, V., Smith, J. T., Waegemann, K., Mokranjac, D., *et al.* (2015) Functional complementation analyses reveal that the single PRAT family protein of *Trypanosoma brucei* is a divergent homolog of Tim17 in *Saccharomyces cerevisiae. Eukaryot. Cell* **14**, 286–296

24. Harsman, A., Oeljeklaus, S., Wenger, C., Huot, J. L., Warscheid, B., and Schneider, A. (2016) The Non-canonical mitochondrial inner membrane presequence translocase of trypanosomatids contains two essential rhomboid-like proteins. *Nat. Commun.* **7**, 13707

25. Singha, U. K., Tripathi, A., Smith, J. T., Jr., Quinones, L., Saha, A., Singha, T., *et al.* (2021) Novel IM-associated protein Tim54 plays a role in the mitochondrial import of internal signal-containing proteins in *Trypanosoma brucei. Biol. Cell* **113**, 39–57

26. Duncan, M. R., Fullerton, M., and Chaudhuri, M. (2013) Tim50 in *Trypanosoma brucei* possesses a dual specificity phosphatase activity and is critical for mitochondrial protein import. *J. Biol. Chem.* **288**, 3184–3197

27. Smith, J. T., Jr., Singha, U. K., Misra, S., and Chaudhuri, M. (2018) Divergent small Tim homologues are associated with TbTim17 and critical for the biogenesis of TbTim17 protein complexes in *Trypanosoma brucei. mSphere* **3**, e00204–e00218

28. Wenger, C., Oeljeklaus, S., Warscheid, B., Schneider, A., and Harsman, A. (2017) A trypanosomal orthologue of an intermembrane space chaperone has a non-canonical function in biogenesis of the single mitochondrial inner membrane protein translocase. *PLoS Pathog.* **13**, e1006550

29. Weems, E., Singha, U. K., Smith, J. T., and Chaudhuri, M. (2017) The divergent N-terminal domain of Tim17 is critical for its assembly in the TIM complex in *Trypanosoma brucei. Mol. Biochem. Parasitol.* **218**, 4–15

30. Singha, U. K., Hamilton, V., and Chaudhuri, M. (2015) Tim62, a Novel mitochondrial protein in *Trypanosoma brucei*, is essential for assembly and stability of the TbTim17 protein complex. *J. Biol. Chem.* **290**, 23226–23239

31. Gentzel, M., Pardo, M., Subramaniam, S., Stewart, A. F., and Choudhary, J. S. (2019) Proteomic navigation using proximity-labeling. *Methods* **164-165**, 67–72

32. Varnaite, R., and MacNeill, S. A. (2016) Meet the neighbors: mapping local protein interactomes by proximity-dependent labeling with Bioid. *Proteomics* **16**, 2503–2518

33. Meyer, K. J., and Shapiro, T. A. (2021) Cytosolic and mitochondrial Hsp90 in cytokinesis, mitochondrial DNA replication, and drug action in *Trypanosoma brucei. Antimicrob. Agents Chemother.* **65**, e0063221

34. Serapian, S. A., Sanchez-Martin, C., Moroni, E., Rasola, A., and Colombo, G. (2021) Targeting the mitochondrial chaperone TRAP1: Strategies and therapeutic perspectives. *Trends Pharmacol. Sci.* **42**, 566–576

35. Dekker, F. A., and Rudiger, S. G. D. (2021) The mitochondrial Hsp90 TRAP1 and Alzheimer's disease. *Front. Mol. Biosci.* **8**, 697913

36. Xie, S., Wang, X., Gan, S., Tang, X., Kang, X., and Zhu, S. (2020) The mitochondrial chaperone TRAP1 as a candidate target of oncotherapy. *Front. Oncol.* **10**, 585047

37. Guzzo, G., Sciacovelli, M., Bernardi, P., and Rasola, A. (2014) Inhibition of succinate dehydrogenase by the mitochondrial chaperone TRAP1 has anti-oxidant and anti-apoptotic effects on tumor cells. *Oncotarget* **5**, 11897–11908

38. Yoshida, S., Tsutsumi, S., Muhlebach, G., Sourbier, C., Lee, M. G., Lee, S., *et al.* (2013) Molecular chaperone TRAP1regulates a metabolic switch between mitochondrial respiration and aerobic glycolysis. *Proc. Natl. Acad. Sci. U. S. A.* **110**, E1604–E1612

39. Joshi, A., Dai, L., Liu, Y., Lee, J., Ghahhari, N. M., Segala, G., *et al.* (2020) The mitochondrial Hsp90 paralog TRAP1 forms an OXPHOS-regulated tetramer and is involved in mitochondrial metabolic homeostasis. *BMC Biol.* **18**, 10

40. Wickner, S., Nguyen, T. L., and Genest, O. (2021) The bacterial Hsp90 chaperone: cellular functions and mechanism of action. *Ann. Rev. Microbiol.* **75**, 719–739

41. Sato, T., Minagawa, S., Kojima, E., Okamoto, N., and Nakamoto, H. (2010) HtpG, the prokaryotic homologue of Hsp90, stabilizes a phyco-bilisome protein in the cyanobacterium synechococcus elongatus PCC 7942. *Mol. Microbiol.* **76**, 576–589

42. Meier, S., Neupert, W., and Herrmann, J. M. (2005) Conserved N-terminal negative charges in the Tim17 subunit of the TIM23 translocase play a critical role in the import of preproteins into mitochondria. *J. Biol. Chem.* **280**, 7777–7785

43. Mani, J., Rout, S., Desy, S., and Schneider, A. (2017) Mitochondrial protein import - functional analysis of the highly diverged Tom22 orthologue of *Trypanosoma brucei. Sci. Rep.* **7**, 40738

44. Trikin, R., Doiron, N., Hoffmann, A., Haenni, B., Jakob, M., Schnaufer, A., *et al.* (2016) TAC102 is a novel component of the mitochondrial genome segregation machinery in trypanosomes. *PLoS Pathog.* **12**, e1005586

45. Morriswood, B., Havlicek, K., Demmel, L., Yavuz, S., Sealey-Cardona, M., Vidilaseris, K., *et al.* (2013) Novel bilobe components in *Trypanosoma brucei* identified using proximity-dependent biotinylation. *Eukaryote. Cell* **12**, 356–367

46. Zhang, Q., Chen, W., Zhang, B., Li, C., Zhang, X., Wang, Q., *et al.* (2021) Central role of TRAP1 in the ameliorative effect of oleanolic acid on the mitochondrial-mediated and endoplasmic reticulum stress-excitated apoptosis induced by ochratoxin A. *Toxicology* **450**, 152681

47. Sinclair-Davis, A. N., McAllaster, M. R., and de Graffenried, C. L. (2017) A functional analysis of TOEFAZ1 uncovers protein domains essential for cytokinesis in *Trypanosoma brucei. J. Cell Sci.* **130**, 3918–3932

48. Schock, M., Schmidt, S., and Ersfeld, K. (2021) Novel cytoskeleton-associated proteins in *Trypanosoma brucei* are essential for cell morphogenesis and cytokinesis. *Microorganisms* **9**, 2234

49. De Pablos, L. M., Kelly, S., Nascimento, J. de F., Sunter, J., and Carrington, M. (2017) Characterization of RBP9 and RBP10, two developmentally regulated RNA-binding proteins in *Trypanosoma brucei. Open Biol.* **7**, 160159

50. Bastin, P., Ellis, K., Kohl, L., and Gull, K. (2000) Flagellum ontogeny in trypanosomes studied *via* an inherited and regulated RNA interference system. *J. Cell Sci.* **113**, 3321–3328

ASBMB

51. Alsford, S., and Horn, D. (2008) Single-locus targeting constructs for reliable regulated RNAi and transgene expression in *Trypanosoma brucei*. *Mol. Biochem. Parasitol.* **161**, 76–79

52. Chaudhuri, M., Ajayi, W., and Hill, G. C. (1998) Biochemical and molecular properties of the *Trypanosoma brucei* alternative oxidase. *Mol. Biochem. Parasitol.* **95**, 53–68

53. Effron, P. N., Torri, A. F., Engman, D. M., Donelson, J. E., and Englund, P. T. (1993) A mitochondriak heat shock protein from *Crithidia fasiculata*. *Mol. Biochem. Parasitol.* **59**, 191–200

54. Singha, U. K., Peprah, E., Williams, S., Walker, R., Saha, L., and Chaudhuri, M. (2008) Characterization of the mitochondrial inner membrane protein translocator Tim17 from Trypanosoma brucei. *Mol. Biochem. Parasitol.* **159**, 30–43

55. Chaudhuri, M. (2001) Cloning and characterization of a novel serine/threonine protein phosphatase type 5 from *Trypanosoma brucei. Gene* **266**, 1–13

56. Sharma, S., Singha, U. K., and Chaudhuri, M. (2010) Role of Tob55 on mitochondrial protein biogenesis in Trypanosoma brucei. *Mol. Biochem. Parasitol.* **174**, 89–100

57. Lin, A. J., Fng, J., Schieltz, D. M., Carmack, E., Mize, G. J., Morris, s DR., *et al*. (1999) Direct analysis of protein complexes using mass spectrometry. *Nat. Biotechnol.* **17**, 676–682